THE JOURNAL OF PHYSICAL CHEMISTRY Letters

Letter

pubs.acs.org/JPCL

Vibrational Dynamics of a Perylene–Perylenediimide Donor–Acceptor Dyad Probed with Femtosecond Stimulated Raman Spectroscopy

Kristen E. Brown, Brad S. Veldkamp, Dick T. Co,* and Michael R. Wasielewski*

Department of Chemistry and Argonne-Northwestern Solar Energy Research (ANSER) Center, Northwestern University, Evanston, Illinois 60208-3113, United States

Supporting Information

ABSTRACT: The ultrafast vibrational dynamics of the photoinduced charge-transfer reaction between perylene (Per) and perylene-3,4:9,10-bis(dicarboximide) (PDI) were investigated using femtosecond stimulated Raman spectroscopy (FSRS). Specifically probing the structural dynamics of PDI following its selective photoexcitation in a covalently linked dyad reveals vibrational modes uniquely characteristic to the PDI lowest excited singlet state and radical anion between 1000 and 1700 cm^{-1}. A comparison of these vibrations to those of the ground state reveals the appearance of new ^{1}*PDI and $PDI^{-\bullet}$ stretching modes in the dyad at 1593 and 1588 cm^{-1}, respectively. DFT calculations reveal that these vibrations are parallel to the long axis of PDI and thus then may be integral to the charge separation reaction. The ability to differentiate excited state from radical anion vibrational modes allows the evaluation of the influence of specific modes on the charge transfer dynamics in donor–bridge–acceptor systems based on PDI molecular constructs.

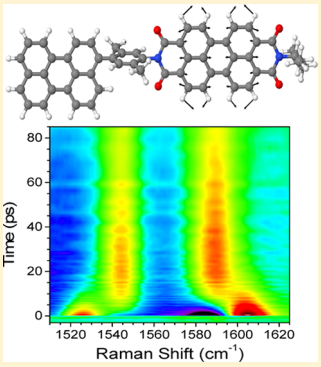

SECTION: Spectroscopy, Photochemistry, and Excited States

The rational design of efficient artificial photosynthetic systems capable of mimicking electron transfer reactions in nature requires a fundamental understanding of light-harvesting, charge separation (CS), and charge transport. Although various covalent donor–acceptor systems have been developed to address each of these challenges in artificial photosynthesis,[1−6] it is often unclear how nuclear motions within these complexes promote electron transfer. In addition, as complex systems capable of self-ordering and self-assembling are developed for the conversion of photon energy to stored charges, understanding the contributions of nuclear motions to energy-wasting charge recombination (CR) processes becomes equally important.[1] For example, these considerations play an important role in donor-bridge-acceptor systems being implemented in solar energy conversion technologies such as dye-sensitized solar cells.[7] Time-resolved vibrational spectroscopy allows for the interrogation of structural changes that occur during these processes, which are difficult to resolve using transient absorption techniques. The recent development of femtosecond stimulated Raman spectroscopy (FSRS) overcomes several limitations of other vibrational spectroscopy techniques because it is insensitive to fluorescence or scattering, has high spectral (~10 cm^{-1}) and temporal (~60 fs) resolution, and is self-phase matched.[8,9] Recently, Fujisawa et al. demonstrated the use of FSRS to evaluate the structural dynamics of a noncovalently bound charge-transfer complex.[10]

To explore the charge-transfer structural dynamics in artificial photosynthetic systems, we synthesized a model electron donor–acceptor dyad using perylene-3,4:9,10-bis(dicarboximide) (PDI) as the acceptor and perylene (Per) as the donor. PDI and its derivatives are commonly utilized as chromophores for solar energy conversion systems due to their strong visible light absorption, thermal stability, and advantageous self-assembly properties.[2,11] The photoinduced dynamics of monomeric PDI (PDI-Xy) and a linear donor–acceptor dyad (PDI-Xy-Per, Chart 1) were probed using FSRS. Whereas time-resolved resonance Raman experiments have been used to interrogate the excited state dynamics of Per,[12] they have not yet been applied to PDI or to any electron donor–acceptor systems based on PDI. In the work presented here, photo-

Chart 1. Structures of PDI-Xy (top) and PDI-Xy-Per (bottom)

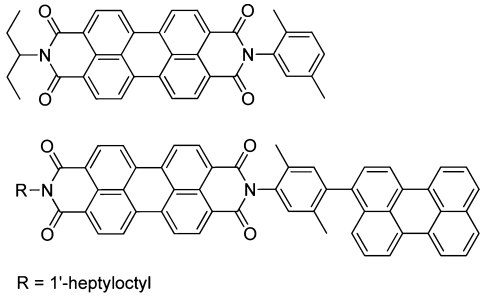

Received: August 3, 2012
Accepted: August 8, 2012
Published: August 8, 2012

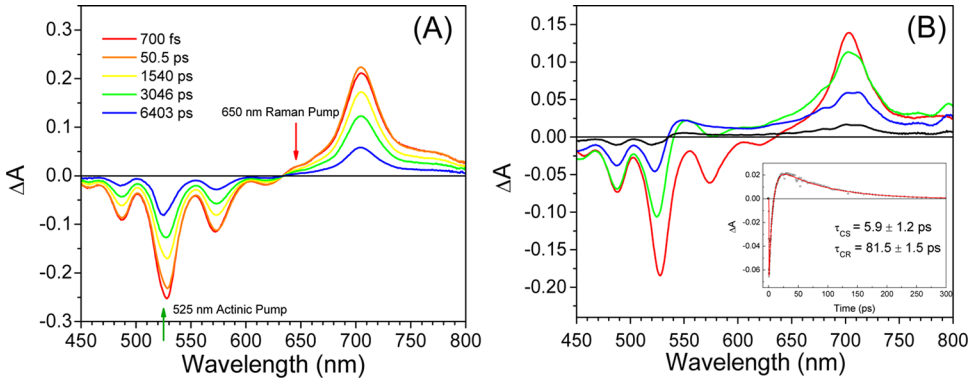

Figure 1. fsTA spectra of PDI-Xy (A) and PDI-Xy-Per (B) in CH_2Cl_2. (A) PDI-Xy decays monoexponentially with τ_{ESD} = 3700 ± 400 ps. Arrows indicate actinic pump and Raman pump excitation wavelengths for both PDI-Xy and PDI-Xy-Per. (B) PDI-Xy-Per charge transfers to $PDI^{-\bullet}$-Xy-$Per^{+\bullet}$ in τ_{CS} = 6 ± 1 ps and recombines with τ_{CR} = 82 ± 2 ps. Inset shows kinetics and fit at 575 nm.

excitation of the PDI moiety within PDI-Xy-Per resulted in the appearance of new vibrational modes, which are distinctly coupled to the CS reaction. The results also demonstrate how FSRS can be used to unambiguously differentiate the excited state from the charge-separated state of common organic chromophores. It is well-known that the $S_n \leftarrow S_1$ electronic absorption spectra of polycyclic aromatic molecules frequently strongly overlap with those of the corresponding radical anions.

The syntheses of PDI-Xy and PDI-Xy-Per are outlined in the Supporting Information. As a control, PDI-Xy radical anion was generated in CH_2Cl_2 using a solution of cobaltocene ($E_{1/2}^{0/+}$ = −1.33 V vs $FeCp_2^{0/+}$ in CH_2Cl_2)[13,14] in a nitrogen atmosphere glovebox.

Femtosecond transient absorption (fsTA) was employed to first obtain the excited electronic state dynamics, namely, the CS and CR rates, as well as to determine the appropriate Raman pump wavelength to leverage resonance enhancement of the Raman effect. Photoexcitation of PDI-Xy in CH_2Cl_2 at its $S_1 \leftarrow S_0$ transition (525 nm, 0.6 μJ/pulse, Figure 1) results in the instrument-limited appearance of the ^{1}*PDI transient absorption spectrum (λ_{max} = 700 nm), which decays with τ = 3.7 ± 0.4 ns. Selective photoexcitation of PDI within PDI-Xy-Per at 525 nm results in the instrument-limited formation of ^{1}*PDI, followed by CS to form $PDI^{-\bullet}$-Xy-$Per^{+\bullet}$ with τ_{CS} = 6 ± 1 ps, as monitored by the formation of $Per^{+\bullet}$ at 550 nm coincident with decay of the ^{1}*PDI stimulated emission at 575 nm. In addition, as CS produces $PDI^{-\bullet}$, the initial absorption at 700 nm broadens.[15,16] $PDI^{-\bullet}$-Xy-$Per^{+\bullet}$ recombines to the ground state with τ_{CR} = 82 ± 2 ps.

To probe the CS vibrational dynamics, we examined PDI-Xy and PDI-Xy-Per using FSRS. A detailed description of the FSRS and fsTA experimental setup is available in the Supporting Information as well as the kinetic analyses of the PDI-Xy and PDI-Xy-Per data. In brief, FSRS uses three pulses generated from the output of a Ti:Sapphire regeneratively amplified laser system. A tunable actinic pump (525 nm, 0.5 μJ/pulse) generates ^{1}*PDI. Picosecond (650 nm, 0.6 μJ/pulse) and femtosecond broadband (white light) probe pulses stimulate the Raman transition. Temporal resolution (300 fs by optical Kerr effect cross correlation measurements) is determined by the convolution of the femtosecond actinic and white-light probe pulses, the latter of which gates the Raman scattering. High spectral resolution results from the narrow bandwidth (15 cm^{-1}) of the Raman pump pulse. Use of the 650 nm Raman pump selects against resonance with absorption features from $Per^{+\bullet}$ (460 to 580 nm)[17] and is far removed from the ground-state transition. Resonance-enhancement of the excited state and radical anion also ensures that modes relevant to the electron transfer process are being probed.[18] The fsTA experiments utilize only the actinic and white-light probe pulses.

Figure 2A,B displays selected FSRS spectra of PDI-Xy and PDI-Xy-Per, respectively, in CH_2Cl_2 as well as their respective resonance-enhanced ground-state spectra (Raman pump at 550 nm, bottom traces). The ground-state and excited-state spectra in Figure 2 are the result of subtracting a CH_2Cl_2 spectrum as well as a spline-fit broad baseline. A full description of the

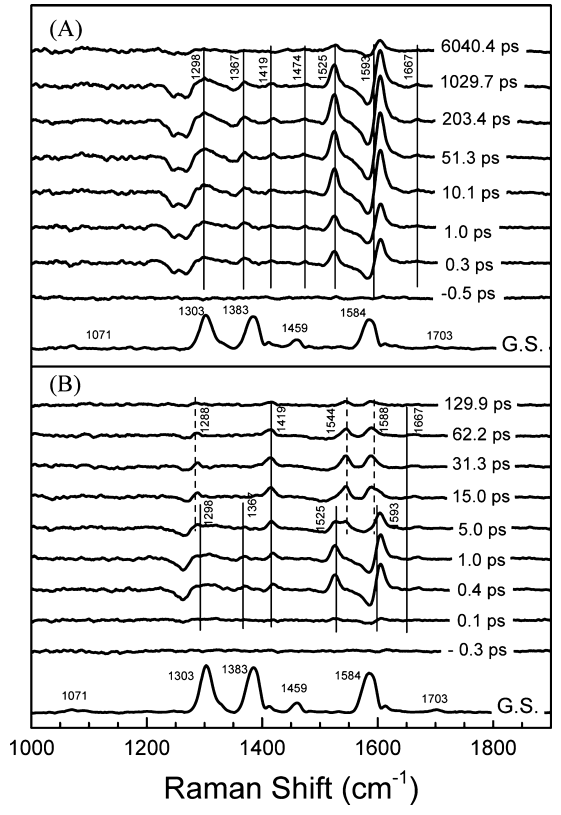

Figure 2. Time-resolved FSRS data and the resonance-enhanced ground state Raman spectra of (A) PDI-Xy and (B) PDI-Xy-Per in CH_2Cl_2. Solid lines designate the evolution of ^{1}*PDI modes, whereas $PDI^{-\bullet}$ modes are labeled with dotted lines.

dx.doi.org/10.1021/jz301107c | J. Phys. Chem. Lett. 2012, 3, 2362−2366

Table 1. Observed and Theoretical Vibrational Frequencies (cm^{-1})

PDI-Xy						PDI-Xy-Per		
ground state	calcd	^{1}*PDI-Xy	calcd[a]	$PDI^{-\bullet}$-Xy	calcd	ground state	^{1}*PDI-Xy-Per	$PDI^{-\bullet}$-Xy- $Per^{+\bullet}$
1071	[c]					1071		
1303	1303	1298[b]	1301	1290	1273	1303	1298[b]	1288
1383	1379	1367	1359			1383	1367	
1459	1442	1419	1453	1419	1445	1459	1419	1419
		1474	[c]				1474	[c]
1584	1586	1525	1529	1542	1541	1584	1525	1544
		1593[b]	1599	1585	1584		1593[b]	1588
1703	1712	1677				1703	1677	1677

[a] ^{1}*PDI-Xy calculated frequencies are based on values derived using Me-PDI-Me. [b] Peak values are assigned using the average between the maximum and minimum peak values. [c] No strongly correlated calculated match was found for this mode due to its low intensity.

baseline subtraction and kinetic evaluation is available in the Supporting Information. The ground-state spectrum of PDI-Xy displays six vibrational modes between 1050 and 1710 cm^{-1} (Figure 2A, bottom trace). The three most intense Raman bands at 1303, 1383, and 1584 cm^{-1} correspond to in-plane C═C stretching frequencies of the perylene aromatic core and have been observed[12] and calculated[19] in previous Raman studies of Per as well as in single molecule surface-enhanced resonance Raman scattering experiments of PDI.[20] Evaluation of the ground-state spectrum of PDI-Xy-Per reveals identical core stretches (Figure 2B, bottom trace) to PDI-Xy, indicating limited vibrational coupling between Per and PDI-Xy.

Selective photoexcitation of PDI within PDI-Xy-Per (Figure 2B) results in the growth of sharp peaks, identical to observed ^{1}*PDI-Xy modes (Figure 2A). A comparison between the ground- and excited-state spectra of both PDI-Xy-Per and PDI-Xy reveals a clear downshift of the frequencies upon excitation (Table 1). This is supported using theoretical vibrational calculations (see below). Notably, two of the observed modes, 1298 and 1593 cm^{-1}, show dispersive character. Because of this dispersion, peak assignments were determined based on the average of the maximum and minimum peak values. This dispersion was shown to persist for the duration of the stimulated emission and is wavelength-specific (Figure S8 in the Supporting Information), suggesting a contribution from third order terms resulting from resonance contributions from both $S_1 \rightarrow S_0$ as well as $S_n \leftarrow S_1$.[21] This explanation is consistent with the lack of dispersion observed once PDI has charge-transferred to $PDI^{-\bullet}$-Xy-$Per^{+\bullet}$ (see below). The excited-state Raman data also reveal that the peak at 1593 cm^{-1} does not correspond to any Raman active modes observed in the resonance Raman ground-state spectrum. Theoretical calculations described below aid in structural assignments of the observed modes.

Figure 2B displays the FSRS data and resonance-enhanced ground-state data of PDI-Xy-Per. As CS occurs to form $PDI^{-\bullet}$-Xy-$Per^{+\bullet}$, anion peaks at 1288, 1419, 1544, and 1588 cm^{-1} emerge. These values were compared with a resonance-enhanced spectrum (Raman pump = 650 nm) of chemically reduced PDI using cobaltocene in CH_2Cl_2 (Figures S5 and S7 in the Supporting Information).[16,22] The slight frequency difference between the chemically reduced PDI-Xy anion modes and the observed $PDI^{-\bullet}$-Xy-$Per^{+\bullet}$ stretches are assumed to be within the error of our experiment and cannot be assigned to significant structural changes in the perylene core of PDI (Table 1). These peaks are observed to decay on the time scale of CR. It is apparent in Figure 2B that as the S_1 peaks at 1525 and 1593 cm^{-1} decay, two peaks unique to the radical anion (1544 and 1588 cm^{-1}) arise. Dynamics were evaluated using a single-frequency fit at the maximum peak values of the four observed modes. Figure 3 displays kinetics acquired at 1605

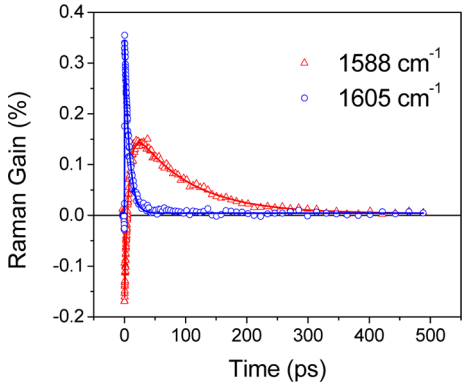

Figure 3. Single-wavenumber kinetics measured at 1588 (△) and 1605 cm^{-1} (○).

and 1588 cm^{-1}. 1605 cm^{-1} corresponds to the maximum value of the peak previously assigned as 1593 cm^{-1} based on its dispersive character. Kinetics acquired at 1605 cm^{-1} correspond to the quenching of ^{1}*PDI as charge transfer occurs to form $PDI^{-\bullet}$-Xy-$Per^{+\bullet}$ with $\tau_{CS} = 7.5 \pm 0.2$ ps. The complete decay of this peak to baseline confirms that it is uniquely attributable to ^{1}*PDI. Comparison with the observed mode at 1588 cm^{-1} shows an increase as CS occurs, followed by a decay to baseline, $\tau_{CR} = 90 \pm 2$ ps. The initial negative amplitude is due to the dispersive nature of the excited-state peak. Notably, the frequency shifts associated with the formation of the radical ion pair differ for each mode. The 1525 and 1593 cm^{-1} modes are observed to shift in opposite directions upon CS. This phenomenon is consistent throughout several solvents.[23]

To aid with assignment of these modes, we have calculated Raman frequencies (DFT B3LYP/6-31G*) of the ground, excited, and anion states of PDI.[24] The ground-state and anion frequencies were calculated using geometry optimized PDI-Xy. To reduce computational time, we calculated the excited-state frequencies using methyl (Me) groups on the imide positions (Supporting Information). The calculated frequencies for each state effectively match the observed vibrational frequencies after a scaling factor of 0.97 is applied (Table 1). On the basis of the output of these results, we can conclude that the 1584 cm^{-1} PDI-Xy ground-state mode downshifts to 1525 cm^{-1} after photexcitation and increases to 1542 cm^{-1} upon the formation of the anion. The ^{1}*PDI and $PDI^{-\bullet}$ modes at 1593 and 1588

dx.doi.org/10.1021/jz301107c | J. Phys. Chem. Lett. 2012, 3, 2362−2366

cm^{-1}, respectively, do not correspond to modes that are observed in the ground state (Figure 4). The presence of this

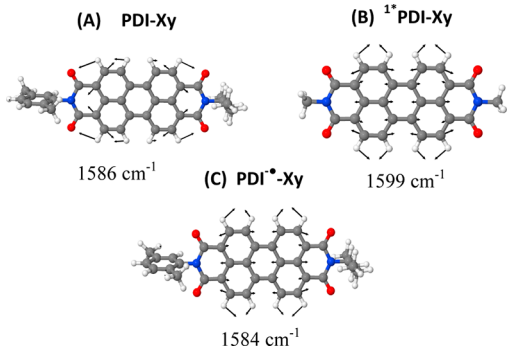

Figure 4. Contributing vibrational modes and calculated frequencies of (A) PDI ground state, (B) ^{1}*PDI, and (C) PDI$^{-\bullet}$.

stretch in both the excited state and the anion, which comprise nuclear motions largely parallel to the long-axis of PDI (versus stretches composed of perpendicular stretching motions), not only suggests that the electronic distributions on the excited state and the anion are similar but also implies that an additional vibration is coupled to the charge-transfer process.

Evaluation of the PDI-Xy-Per electron-transfer dyad with FSRS has revealed structural information on the nature of the charge-transfer processes between PDI and Per that are not available using fsTA. Using FSRS, we have demonstrated the ability to differentiate between ^{1}*PDI and PDI$^{-\bullet}$. Following photoexcitation of PDI, unique excited-state modes appear between 1200 and 1700 cm^{-1}. As CS occurs, the observed peaks decay, giving rise to PDI$^{-\bullet}$ vibrations. The presence of the new Raman-active stretch at 1593 (^{1}*PDI) and 1588 cm^{-1} (PDI$^{-\bullet}$) that is present only in the dyad suggests that additional vibrations are necessary to mediate CS. The ability to observe structural changes among the ground, excited, and anion states of PDI opens the door to interrogate several structure–function relationships. Specifically, FSRS is capable of elucidating the dynamics of ultrafast charge transfer and delocalization, which makes it possible to understand the electronic and vibrational coupling between adjacent chromophores. This can be applied to discrete dimer systems and self-assembled structures in solution as well as in thin films to interrogate exciton formation and subsequent splitting to generate free charge carriers in systems beyond PDI.

■ ASSOCIATED CONTENT

Ⓢ Supporting Information

Experimental procedure, additional figures, detailed calculations, and full citation for ref 24. This material is available free of charge via the Internet at http://pubs.acs.org.

■ AUTHOR INFORMATION

Corresponding Author

*E-mail: co@northwestern.edu, m-wasielewski@northwestern.edu.

Notes

The authors declare no competing financial interest.

■ ACKNOWLEDGMENTS

We would like to thank Drs. Torsten Fiebig, Renee Frontiera, and Ryan Young for numerous helpful discussions. This work was supported by the Chemical Sciences, Geosciences, and Biosciences Division, Office of Basic Energy Sciences, DOE under grant no. DE-FG02-99ER14999. D.T.C. acknowledges funding from the Initiative for Sustainability and Energy at Northwestern (ISEN). B.S.V. is supported by the Department of Energy Office of Science Graduate Fellowship Program (DOE SCGF), made possible in part by the American Recovery and Reinvestment Act of 2009, administered by ORISE-ORAU under contract no. DE-AC05-06OR23100.

■ REFERENCES

(1) Wasielewski, M. R. Self-Assembly Strategies for Integrating Light Harvesting and Charge Separation in Artificial Photosynthetic Systems. *Acc. Chem. Res.* **2009**, *42*, 1910–21.
(2) Wasielewski, M. R. Energy, Charge, and Spin Transport in Molecules and Self-Assembled Nanostructures Inspired by Photosynthesis. *J. Org. Chem.* **2006**, *71*, 5051–5066.
(3) Magnuson, A.; Anderlund, M.; Johansson, O.; Lindblad, P.; Lomoth, R.; Polivka, T.; Ott, S.; Stensjö, K.; Styring, S.; Sundström, V.; et al. Biomimetic and Microbial Approaches to Solar Fuel Generation. *Acc. Chem. Res.* **2009**, *42*, 1899–1909.
(4) Gust, D.; Moore, T. A.; Moore, A. L. Solar Fuels Via Artificial Photosynthesis. *Acc. Chem. Res.* **2009**, *42*, 1890–1898.
(5) McConnell, I.; Li, G.; Brudvig, G. W. Energy Conversion in Natural and Artificial Photosynthesis. *Chem. Biol.* **2010**, *17*, 434–447.
(6) Kalyanasundaram, K.; Graetzel, M. Artificial Photosynthesis: Biomimetic Approaches to Solar Energy Conversion and Storage. *Curr. Opin. Biotechnol.* **2010**, *21*, 298–310.
(7) Yella, A.; Lee, H.-W.; Tsao, H. N.; Yi, C.; Chandiran, A. K.; Nazeeruddin, M. K.; Diau, E. W.-G.; Yeh, C.-Y.; Zakeeruddin, S. M.; Grätzel, M. Porphyrin-Sensitized Solar Cells with Cobalt (II/III)–Based Redox Electrolyte Exceed 12% Efficiency. *Science* **2011**, *334*, 629–634.
(8) Frontiera, R. R.; Mathies, R. A. Femtosecond Stimulated Raman Spectroscopy. *Laser Photonics Rev.* **2011**, *5*, 102–113.
(9) Rhinehart, J. M.; Mehlenbacher, R. D.; McCamant, D. Probing the Charge Transfer Reaction Coordinate of 4-(Dimethylamino)-benzonitrile with Femtosecond Stimulated Raman Spectroscopy. *J. Phys. Chem. B* **2010**, *114*, 14646–14656.
(10) Fujisawa, T.; Creelman, M.; Mathies, R. A. Structural Dynamics of a Noncovalent Charge Transfer Complex from Femtosecond Stimulated Raman Spectroscopy. *J. Phys. Chem. B* **2012**. DOI: 10.1021/jp3001306.
(11) Wurthner, F. Perylene Bisimide Dyes as Versatile Building Blocks for Functional Supramolecular Architectures. *Chem. Commun.* **2004**, 1564–1579.
(12) Matsunuma, S.; Akamatsu, N.; Kamisuki, T.; Adachi, Y.; Maeda, S.; Hirose, C. S[Sub N] <– S[Sub 1] and S[Sub 1] –> S[Sub 0] Resonance Cars Spectra of Perylene in the S[Sub 1] State. *J. Chem. Phys.* **1988**, *88*, 2956–2961.
(13) Connelly, N. G.; Geiger, W. E. Chemical Redox Agents for Organometallic Chemistry. *Chem. Rev.* **1996**, *96*, 877–910.
(14) An, Z.; Odom, S. A.; Kelley, R. F.; Huang, C.; Zhang, X.; Barlow, S.; Padilha, L. A.; Fu, J.; Webster, S.; Hagan, D. J.; et al. Synthesis and Photophysical Properties of Donor- and Acceptor-Substituted 1,7-Bis(arylalkynyl)perylene-3,4:9,10-bis(dicarboximide)s. *J. Phys. Chem. A* **2009**, *113*, 5585–5593.
(15) Giaimo, J. M.; Lockard, J. V.; Sinks, L. E.; Scott, A. M.; Wilson, T. M.; Wasielewski, M. R. Excited Singlet States of Covalently Bound, Cofacial Dimers and Trimers of Perylene-3,4:9,10-bis(dicarboximide)-s. *J. Phys. Chem. A* **2008**, *112*, 2322–2330.
(16) Gosztola, D.; Niemczyk, M. P.; Svec, W.; Lukas, A. S.; Wasielewski, M. R. Excited Doublet States of Electrochemically Generated Aromatic Imide and Diimide Radical Anions. *J. Phys. Chem. A* **2000**, *104*, 6545–6551.
(17) Kimura, K.; Yamazaki, T.; Katsumata, S. Dimerization of the Perylene and Tetracene Radical Cations and Electronic Absorption Spectra of Their Dimers. *J. Phys. Chem.* **1971**, *75*, 1768–1774.

(18) Barbara, P. F.; Meyer, T. J.; Ratner, M. A. Contemporary Issues in Electron Transfer Research. *J. Phys. Chem.* **1996**, *100*, 13148−13168.
(19) Ong, K. K.; Jensen, J. O.; Hameka, H. F. Theoretical Studies of the Infrared and Raman Spectra of Perylene. *THEOCHEM* **1999**, *459*, 131−144.
(20) Tolaieb, B.; Constantino, C. J. L.; Aroca, R. F. Surface-Enhanced Resonance Raman Scattering as an Analytical Tool for Single Molecule Detection. *Analyst* **2004**, *129*, 337−341.
(21) Niu, K.; Zhao, B.; Sun, Z.; Lee, S.-Y. Analysis of Femtosecond Stimulated Raman Spectroscopy of Excited-State Evolution in Bacteriorhodopsin. *J. Chem. Phys.* **2010**, *132*, 084510−9.
(22) An, Z.; Odom, S. A.; Kelley, R. F.; Huang, C.; Zhang, X.; Barlow, S.; Padilha, L. A.; Fu, J.; Webster, S.; Hagan, D. J.; et al. Synthesis and Photophysical Properties of Donor- and Acceptor-Substituted 1,7-Bis(arylalkynyl)perylene-3,4:9,10-bis(dicarboximide)s. *J. Phys. Chem. A* **2009**, *113*, 5585−5593.
(23) Dynamics were explored in CH_2Cl_2, THF, CD_2Cl_2, and CCl_4. These solvents were chosen based on their optical window as well as their respective dielectric constants.
(24) Shao, Y.; Molnar, L. F.; Jung, Y.; Kussmann, J.; Ochsenfeld, C.; Brown, S. T.; Gilbert, A. T. B.; Slipchenko, L. V.; Levchenko, S. V.; O'Neill, D. P.; et al. Advances in Methods and Algorithms in a Modern Quantum Chemistry Program Package. *Phys. Chem. Chem. Phys.* **2006**, *8*, 3172−3191.